PHYSICAL REVIEW B
CONDENSED MATTER

THIRD SERIES, VOLUME 40, NUMBER 11 15 OCTOBER 1989-I

Temperature dependence of sound attenuation in impure metals

M. Yu. Reizer
Department of Applied Physics, Stanford University, Stanford, California 94305-4090
(Received 3 April 1989)

Temperature dependence of the sound-attenuation coefficient in an impure metal arising from inelastic electron scattering is investigated. We consider the electron-phonon and electron-electron interactions, as well as the electron-magnon interaction in a ferromagnetic metal, as processes of inelastic electron scattering. The interference effects between inelastic electron scattering and the elastic electron-impurity scattering, together with the weak-localization effect, are taken into account.

I. INTRODUCTION

The attenuation of sound in impure metals due to the electron-phonon interaction was calculated by Pippard[1] by means of the quasiclassical Boltzmann equation. The results obtained there were then confirmed by microscopic calculations by Schmid[2] and by Grunewald and Sharnberg.[3] According to Refs. 1–3, the attenuation coefficient depends essentially on the parameter kl, where k is the wave vector of the sound phonon and l is the electron mean free path due to the electron-impurity scattering: $l=v_F\tau$, where v_F is the Fermi velocity and τ is the electron-momentum relaxation time. For $kl \gg 1$ the attenuation is proportional to k and does not depend on τ (the collisionless regime). For $kl \ll 1$ (hydrodynamic regime) the attenuation coefficients for longitudinal and transverse phonons are

$$\gamma^l=\frac{4}{15}\frac{Zm}{M}(kv_F)^2\tau, \quad \gamma^t=\tfrac{3}{4}\gamma^l , \tag{1}$$

where m,M are the electron and ion masses, and Z is the average charge per unit cell, which is determined from the equation

$$n_e=Z_{\rm ion}N_{\rm ion}+Z_{\rm imp}N_{\rm imp}=ZN . \tag{2}$$

Here, $Z_{\rm ion}$ and $Z_{\rm imp}$ are the valences of the host ion and the impurity ion, respectively; $N_{\rm ion}$ and $N_{\rm imp}$ are their concentrations.

The temperature dependence of the attenuation arises only from inelastic electron scattering. The effect of the electron–thermal-phonon scattering on the sound attenuation was considered in Ref. 4. The electron-phonon and electron-impurity scattering processes were treated independently, that is, equivalent to Matthiessen's rule for the resistivity. The validity of such an approach for both the resistivity and the sound attenuation requires some justification.

Note that even in relatively pure samples under the experimental conditions of Ref. 5 the electron-impurity scattering is the main electron-momentum relaxation process. This dominance of electron-impurity scattering was exploited in Ref. 6 for obtaining the temperature-dependent corrections to the conductivity for an impure metal due to the electron-electron interaction and in Ref. 7 due to the electron-phonon interaction. It was shown that Matthiessen's rule breaks down at low temperatures when the interference between the electron-electron (electron-phonon) and the electron-impurity interactions becomes essential.

We use the same approach in the present paper to calculate the temperature-dependent corrections $\Delta\gamma$ to the attenuation of sound in an impure metal due to different inelastic-electron-scattering mechanisms and the effects of weak localization.

The paper is organized as follows. In Sec. II we describe the electron-phonon interaction in impure metals. The effective interaction vertices are introduced, which allow us to treat the screening and impurity renormalization effects consistently. We then calculate the corrections to the sound attenuation due to the interaction of electrons with thermal phonons. The influence of the electron-magnon interaction on the sound attenuation in an impure ferromagnetic metal is investigated in Sec. III. In Sec. IV we consider the effects of weak localization and in Sec. V the effects of the Coulomb electron-electron interaction and the electron-electron interaction in the Cooper channel.

The effects of localization and the Coulomb electron-electron interaction on the sound attenuation were investigated recently in many papers.[8–11] In our approach we consider some new diagrams, taking into account the

effect of screening and impurity renormalization, but after some cancellations the final results coincide with Refs. 8–10.

II. ELECTRON-PHONON INTERACTION IN IMPURE METALS

We use the Keldysh-diagrammatic technique for nonequilibrium processes[12] in which the electron and phonon Green's functions, along with the electron and phonon self-energies, are represented by matrices

$$\hat{G}=\begin{bmatrix} 0 & G^A \\ G^R & G^C \end{bmatrix}, \quad \hat{D}=\begin{bmatrix} 0 & D^A \\ D^R & D^C \end{bmatrix}, \qquad \hat{\Sigma}=\begin{bmatrix} \Sigma^C & \Sigma^R \\ \Sigma^A & 0 \end{bmatrix}, \quad \hat{\Pi}=\begin{bmatrix} \Pi^C & \Pi^R \\ \Pi^A & 0 \end{bmatrix}. \tag{3}$$

The electron Green's function averaged over impurity positions equals

$$G^R(\mathbf{p},\varepsilon)=[G^A(\mathbf{p},\varepsilon)]^*=(\varepsilon-\xi_{\mathbf{p}}+i/2\tau)^{-1}, \qquad \xi_{\mathbf{p}}=(p^2-p_F^2)/2m \tag{4}$$

where p_F is the Fermi momentum. In a spatially uniform system

$$G^C(\mathbf{p},\varepsilon)=S(\varepsilon)[G^A(\mathbf{p},\varepsilon)-G^R(\mathbf{p},\varepsilon)], \qquad S(\varepsilon)=-\tanh(\varepsilon/2T). \tag{5}$$

For equilibrium thermal phonons,

$$D^R(\mathbf{q},\omega)=[D^A(\mathbf{q},\omega)]^*=(\omega-\omega_{q,\lambda}+i0)^{-1}-(\omega+\omega_{q,\lambda}+i0)^{-1}, \tag{6}$$

$$D^C(\mathbf{q},\omega)=[2N(\omega)+1][D^R(\mathbf{q},\omega)-D^A(\mathbf{q},\omega)], \qquad N(\omega)=[\exp(\omega/T)-1]^{-1} \tag{7}$$

where $\omega_{q,\lambda}$ is the phonon frequency and λ the polarization index.

The interaction vertices in the Keldysh technique are represented by objects of the form Q_{ij}^l, where the upper index is for bosons, the lower for electrons. The vertex for elastic electron-impurity scattering corresponds to the matrix $(\sigma_x)_{ij}$, where σ_x is a 2×2 Pauli matrix.

To consider the interaction between electrons and both sound and thermal phonons, we work in the frame of reference moving together with the lattice (MFR).[13,14,2] In MFR impurities are motionless, which allows us to neglect inelastic electron-impurity scattering. In describing the vertices of the electron-phonon interaction, we follow Ref. 15. Without screening, the electron-phonon vertex is

$$(\Gamma_0)_{ij}^k=-i\frac{(\mathbf{p}\cdot\mathbf{q})(\mathbf{p}\cdot\mathbf{e}_\lambda)}{m(2MN\omega_{q\lambda})^{1/2}}K_{ij}^k, \tag{8}$$

where $\mathbf{e}_\lambda$ is the polarization vector. The tensor K_{ij}^k is

$$K_{ij}^1=\frac{1}{\sqrt{2}}\delta_{ij}, \quad K_{ij}^2=\frac{1}{\sqrt{2}}(\sigma_x)_{ij}. \tag{9}$$

For longitudinal phonons,

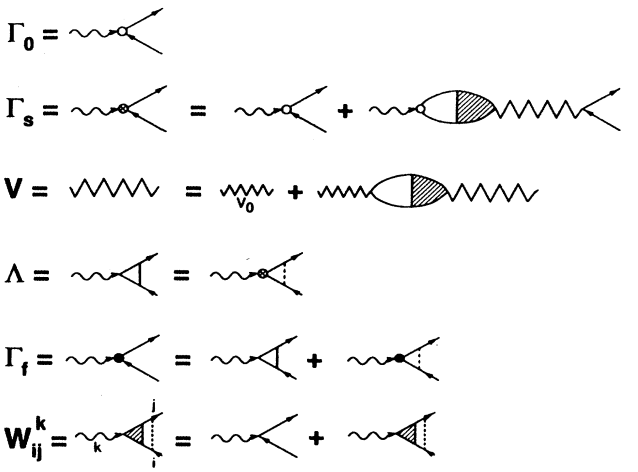

FIG. 1. Γ_0 is the bare electron-phonon vertex, Γ_S is the screened electron-phonon vertex, V is the screened Coulomb potential, V_0 is the Coulomb potential without screening, vertex Λ takes into account the impurity renormalization in the first order of the perturbation theory and vertex Γ_f in all orders, and triangle W represents the scalar vertex renormalized by impurities in the ladder approximation.

$$(\Gamma_0)_{ij}^k=-i3x^2g_{ql}K_{ij}^k, \quad x=\frac{\mathbf{p}\cdot\mathbf{q}}{pq}, \qquad g_{ql}=\frac{2}{3}\frac{\varepsilon_F q}{(2MN\omega_{ql})^{1/2}}. \tag{10}$$

For thermal phonons it is convenient to introduce the dimensionless constant β_l defined by $g_{ql}^2=\beta_l\omega_{ql}\nu^{-1}$, where g_{ql} is given by (10), and

$$\beta_l=\tfrac{2}{3}\varepsilon_F\frac{\nu}{2MNu_l^2}=\frac{1}{2}, \tag{11}$$

where we used $u_l^2=Zmv_F^2/3M$.

Including the screening effects for longitudinal phonons leads to the vertex Γ_s, shown in Fig. 1:

$$(\Gamma_s)_{ij}^2=ig_{ql}K_{ij}^k\left[1-3x^2+\frac{i\omega\tau(\zeta_0^*-3\zeta_2^*)}{1-\zeta_0^*-i\omega\tau\zeta_0^*}\right], \qquad (\Gamma_s)_{11}^1=(\Gamma_s)_{22}^1=-[(\Gamma_s)_{12}^2]^*, \qquad (\Gamma_s)_{12}^1=(\Gamma_s)_{21}^1=-2[2N(\omega)+1]\mathrm{Re}[(\Gamma_s)_{12}^2], \tag{12}$$

where

$$\zeta_n=\frac{1}{\pi\nu\tau}\int d\mathbf{p}\frac{1}{(2\pi)^3}G^A(\mathbf{p},\varepsilon)G^R(\mathbf{p}+\mathbf{q},\varepsilon+\omega)x^n. \tag{13}$$

For $ql\ll1$ and $\omega\tau\ll1$,

$$\zeta_0=1+i\omega\tau-Dq^2\tau, \quad \zeta_1=-\frac{i}{ql}[1-(1-i\omega\tau)\zeta_0], \qquad \zeta_2=\frac{i}{ql}(1-i\omega\tau)\zeta_1, \quad D=v_F^2\tau/3. \tag{14}$$

For $ql\ll1$ and $\omega\tau\ll1$ the vertex Γ_s should be renormalized by the electron-impurity scattering in the ladder approximation. Because the vertex Γ_s contains both the

scalar and the vector ($-3x^2$) parts, the renormalization is performed by introducing the auxiliary vertex Λ_{ij}^k, shown in Fig. 1. The vertex Λ_{ij}^k is scalar and may be renormalized in the usual manner, which leads to the vertex Γ_f

$$
\begin{aligned}
&(\Gamma_f)_{22}^1 \equiv \Gamma = \frac{ig_{ql}}{\sqrt{2}} \frac{\zeta_0^* - 3\zeta_2^*}{1-\zeta_0^* - i\omega\tau\zeta_0^*} = \frac{4ig_{ql}}{5\sqrt{2}} , \\
&(\Gamma_f)_{12}^1 = S(\varepsilon)\Gamma , \quad (\Gamma_f)_{21}^1 = -S(\varepsilon+\omega)\Gamma , \\
&(\Gamma_f)_{11}^1 = [1-2S(\varepsilon)S(\varepsilon+\omega)]\Gamma , \\
&(\Gamma_f)_{11}^2 = [S(\varepsilon+\omega)-S(\varepsilon)]\Gamma , \\
&(\Gamma_f)_{12}^2 = (\Gamma_f)_{21}^2 = (\Gamma_f)_{22}^2 = 0 .
\end{aligned} \tag{15}
$$

Note that expressions (15) are correct for arbitrary relations between ω and Dq^2 (see Ref. 15). Note also that the exact expressions (12) for the vertex $(\Gamma_s)_{ij}^k$ are very important for constructing the vertex $(\Gamma_f)_{ij}^k$. In all other cases for our calculations we will use the following simplified formula:

$$
(\Gamma_s)_{ij}^k = i(1-3x^2)g_{ql}K_{ij}^k . \tag{16}
$$

For further calculations, we also need the vertex $(\Lambda)_{ij}^k$ for $ql \gg 1$. The vertex $(\Lambda)_{ij}^k$ has the same index structure as $(\Gamma_f)_{ij}^k$ and may be obtained from (15) by substituting Γ for Λ, where

$$
\Lambda \equiv \Lambda_{22}^1 = ig_{ql}\frac{\pi}{2^{3/2}ql}, \quad ql \gg 1 . \tag{17}
$$

As was shown in Ref. 7, the screening effects are not essential for thermal transverse phonons for $T > T_1$, where

$$
T_1 = \frac{u_t}{c}(\varepsilon_F \kappa u_t)^{1/2}, \quad \kappa^2 = 4\pi e^2 \nu, \quad Tl \gg u_t , \tag{18}
$$

where c is the velocity of light and u_t is the velocity of transverse sound.

For a metal, $T_1 \approx 0.1$ K. The screening effects are also unimportant for the long-wavelength thermal transverse phonons for which $Tl \ll u_t$. As for the sound transverse phonons, the screening effects are essential only for $kl \gg 1$, and as long as the phonon frequency is not too high.[1,3] Because for sound phonons we assume the condition $kl \ll 1$ to be true and for thermal phonons the condition $ql \gg 1$ to be true, the interaction between electrons and both sound and thermal transverse phonons is described by the bare vertex Γ_0.

The sound attenuation is obtained from the corresponding phonon self-energy

$$
\gamma = -2\,\mathrm{Im}\Pi^R(\mathbf{k},\Omega)|_{\Omega=\omega_{q\lambda}} . \tag{19}
$$

Diagrams contributing to Π^l for longitudinal and to Π^t for transverse sound phonons without inelastic electron processes are shown in Fig. 2 and lead to expressions (1).

Being interested in the temperature-dependent corrections to the sound attenuation $\Delta\gamma^l$ and $\Delta\gamma^t$, we should consider the phonon self-energy diagrams containing the insertion B due to some inelastic electron processes, as shown in Fig. 2. Note that in the diagrams for $\Delta\Pi^l$ both sound-phonon vertices are screened.

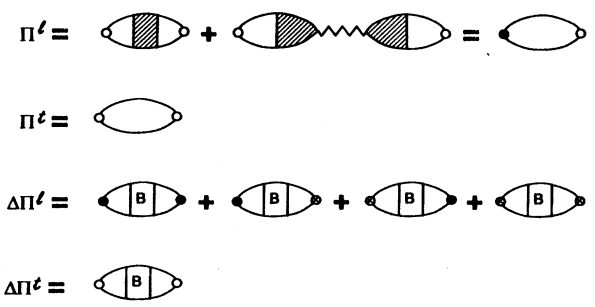

FIG. 2. Π^l and Π^t are the longitudinal- and transverse-phonon self-energies, and $\Delta\Pi^l$ and $\Delta\Pi^t$ are the phonon self-energies, which defined the temperature dependence of the sound attenuation; block B contains some inelastic electron scattering.

Before carrying out the calculation, we identify the essential diagrams for $\Delta\Pi^l$ and $\Delta\Pi^t$. If the sound-phonon vertex Γ_s for longitudinal phonons or the vertex Γ_0 for transverse phonons are separated from another part of the diagram by an impurity line, such a diagram vanishes in the lowest order in kl due to the electron angular integration.

The temperature dependence in $\Delta\Gamma$ is encountered only in the case where $\Delta\Pi$ contains the products $G^C G^C$ or $G^C D^C$. It can be shown[7] that in the first case only the combinations $G^C(\varepsilon)G^C(\varepsilon+\omega+\Omega)$ and $G^C(\varepsilon+\Omega)G^C(\varepsilon+\omega)$ give nonzero contributions, where ω is the frequency of the boson excitation included in the block B.

After expanding in the small frequency range $\Omega \ll \omega, \varepsilon$ and integrating over ε, we find that the temperature dependence of $\Delta\gamma$ is determined by the functions

$$
\begin{aligned}
f(\omega/T) &= \tfrac{1}{2}\int d\varepsilon\, S(\varepsilon+\omega)\frac{\partial S(\varepsilon)}{\partial\varepsilon} \\
&= -\tfrac{1}{2}\int d\varepsilon\, S(\varepsilon)\frac{\partial S(\varepsilon+\omega)}{\partial\varepsilon} \\
&= \frac{\partial}{\partial\omega}[\omega\coth(\omega/2T)] ,
\end{aligned} \tag{20}
$$

$$
\tfrac{1}{2}\int d\varepsilon \frac{\partial S(\varepsilon)}{\partial\varepsilon}(2N_\omega+1) = -\coth(\omega/2T) . \tag{21}
$$

Note that the first combination depends only on the electron temperature and the second on the temperature of the heat bath.

The essential diagrams for $\Delta\Pi_{e\text{-ph}}^l$ determined by the electron–thermal-phonon interaction under the conditions $kl \ll 1$ and $q_T l \gg 1$ ($q_T = T/u$) are shown in Fig. 3.

For the first two diagrams, we define the functions Ψ_1 and Ψ_2, which contain the angular dependence, originating from the vertices Γ_s:

$$
\begin{aligned}
&\Psi_1 = (1-3x^2)(1-3y^2)^2(1-3z^2) , \\
&\Psi_2 = (1-3x^2)^2(1-3y^2)^2 , \\
&x = \frac{\mathbf{p}\cdot\mathbf{k}}{pk}, \quad y = \frac{\mathbf{p}\cdot\mathbf{q}}{pq}, \quad z = \frac{(\mathbf{p}+\mathbf{q})\cdot\mathbf{k}}{|\mathbf{p}+\mathbf{q}|k}
\end{aligned} \tag{22}
$$

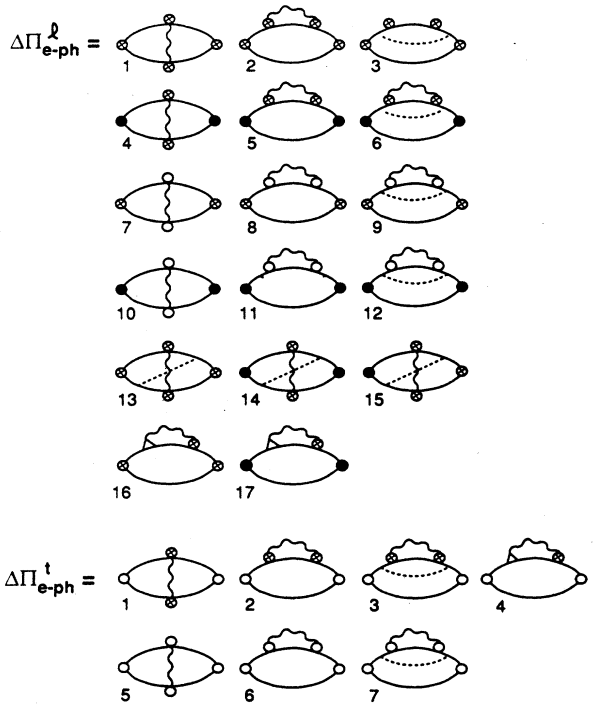

FIG. 3. $\Delta\Pi^{l}_{e\text{-ph}}$ and $\Delta\Pi^{t}_{e\text{-ph}}$ are corrections to the phonon self-energies due to the interaction of electrons with thermal phonons under the conditions $kl \ll 1$ and $ql \gg 1$. For asymmetric graphs, only one diagram is shown.

which holds for $k \ll q$.

If we neglect small terms of order k/p_F and q/p_F, we get $\Psi_1 = \Psi_2 = (1-3x^2)^2(1-3y^2)^2$. Within this approximation, the temperature dependence of the sound attenuation originates from the interference of the electron-phonon and electron-impurity interactions. The contributions of diagrams with all possible orderings of the indices leading to the combination $G^C D^C$ mutually cancel for each diagram of Fig. 3. Only the contributions from diagrams containing the combination $G^C G^C$ remain.

Taking into consideration one longitudinal and two transverse modes of thermal phonons, we have, for the diagrams of Fig. 3,

$$
\begin{aligned}
&(\Delta\gamma^{l}_{e\text{-ph-imp}})_{1-3} = \Delta\gamma^{l} \equiv \frac{4\pi^2}{45}\frac{Zm}{M}(v_F k)^2 \tau \frac{T^2}{\varepsilon_F p_F u_l}\,, \\
&(\Delta\gamma^{l}_{e\text{-ph-imp}})_{4-6} = \tfrac{4}{5}\Delta\gamma^{l}\,, \\
&(\Delta\gamma^{l}_{e\text{-ph-imp}})_{7-9} = -\frac{3}{2}\left[\frac{u_l}{u_t}\right]^3 \Delta\gamma^{l}\,, \\
&(\Delta\gamma^{l}_{e\text{-ph-imp}})_{10-12} = -\frac{6}{5}\left[\frac{u_l}{u_t}\right]^3 \Delta\gamma^{l}\,, \\
&(\Delta\gamma^{l}_{e\text{-ph-imp}})_{13-14} = -\frac{9\pi^4}{10}\Delta\gamma^{l}\,, \\
&(\Delta\gamma^{l}_{e\text{-ph-imp}})_{15} = 0\,, \\
&(\Delta\gamma^{l}_{e\text{-ph-imp}})_{16-17} = -\frac{3\pi^2}{20}\Delta\gamma^{l}\,.
\end{aligned}
\tag{23}
$$

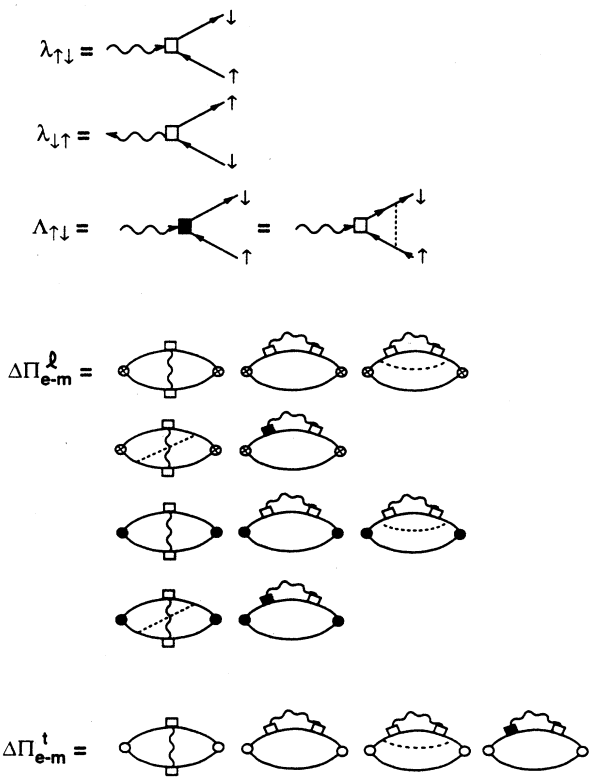

FIG. 4. $\lambda_{\uparrow\downarrow}$ and $\lambda_{\downarrow\uparrow}$ are the bare vertices of the electron-magnon interaction; $\Lambda_{\uparrow\downarrow}$ contains the impurity renormalization in the first order of the perturbation theory. $\Delta\Pi^{l}$ and $\Delta\Pi^{t}$ are corrections to the sound attenuation due to the electron-magnon interaction.

The overall correction to the longitudinal sound attenuation due to the electron-phonon–impurity interference according to (23) is

$$
\Delta\gamma_{e\text{-ph-imp}} = \frac{3}{20}\left[12 - \pi^2 - 6\pi^4 - 18\left[\frac{u_l}{u_t}\right]^3\right]\Delta\gamma^{l}\,. \tag{24}
$$

For transverse sound we take into account the diagrams of Fig. 3 and get

$$
\Delta\gamma^{t}_{e\text{-ph-imp}} = \frac{3}{4}\left[1 - \frac{\pi^2}{4} - \frac{3}{2}\left[\frac{u_l}{u_t}\right]^3\right]\Delta\gamma^{l}\,. \tag{25}
$$

Considering the next term in the expansion of Ψ_1 in the powers of q/p_F, we find

$$
z = x + \frac{\mathbf{q}\cdot\mathbf{k}}{pk} = x + [xy + (1-x^2)^{1/2}(1-y^2)^{1/2}\cos\varphi]\frac{q}{p_F}\,, \tag{26}
$$

where φ is the angle between the projections of vectors $\mathbf{p}$ and $\mathbf{k}$ on the plane perpendicular to $\mathbf{q}$. The angular integration fixes the magnitude $y = -q/2p_F \ll 1$. For transverse sound phonons we take into account the term of order q/p from the vertex Γ_0. It may be shown that the contribution of thermal transverse phonons is negligible. Note also that now both combinations $D^C G^C$ and $G^C G^C$ are important, and finally we get

$$\Delta\gamma^{l}_{e\text{-ph}} = -36\pi\zeta(5)\frac{Zm}{M}(v_F k\tau)^2\frac{T^5}{(p_F u_l)^4}\ ,$$

$$\Delta\gamma^{t}_{e\text{-ph}} = \tfrac{1}{36}\Delta\gamma^{l}_{e\text{-ph}}\ , \qquad (27)$$

where $\zeta(5)\approx 1.03$. Comparison of expressions (24), (25), and (27) with the related results for conductivity[7] shows that the corresponding corrections are proportional: $\Delta\gamma_{e\text{-ph-imp}}\sim\Delta\sigma_{e\text{-ph-imp}}$ and $\Delta\gamma_{e\text{-ph}}\sim\Delta\sigma_{e\text{-ph}}$. The correction $\Delta\gamma_{e\text{-ph-imp}}$ occurs only in an impure metal, while the correction $\Delta\gamma_{e\text{-ph}}$ is similar to results of Ref. 4 for pure metals.

The above calculations refer to the case $q_T l > 1$. For lower temperatures, when $q_T l < 1$, the interaction between electrons and thermal longitudinal phonons is described by vertices Γ_s and Γ_f and for transverse phonons by vertex Γ_0. These do not contain the singular diffusion denominator, unlike the vertex of the electron-electron interaction (see Sec. V). Therefore the corrections to the sound attenuation from the interaction of electrons with thermal phonons for $q_T l < 1$ are negligible in comparison with the corresponding correction from the effects of weak localization (see Sec. IV). A straightforward calculation shows that T^2 terms in $\Delta\gamma_{e\text{-ph-imp}}$ cancel. After expanding the electron Green's functions in powers of $q_T l \ll 1$, we have the final result $\Delta\gamma_{e\text{-ph-imp}}\sim T^4$.

III. IMPURE FERROMAGNETIC METAL

In a ferromagnetic metal the electron-magnon interaction has an effect on the temperature dependence of sound attenuation. The electron-magnon interaction is defined by the s-d exchange Hamiltonian.[16] Taking into account only one-magnon processes, we have

$$H_{s\text{-}d} = -J\left[\frac{2S}{N}\right]^{1/2}\sum_{\mathrm{p,q}}(b_{\mathrm{q}}c^{\dagger}_{\mathrm{p+q}\downarrow}c_{\mathrm{p}\uparrow} + b^{\dagger}_{\mathrm{q}}c^{\dagger}_{\mathrm{p}\uparrow}c_{\mathrm{p+q}\downarrow})\ , \qquad (28)$$

where $b^{\dagger}_{\mathrm{q}}$ and $c^{\dagger}_{\mathrm{p}\uparrow}$ are the magnon and electron creation operators. The arrows in the electron operator stands for the electron spin. J is the exchange integral, and N is the number of magnetic atoms with spin S.

The magnon Green's function and the magnon spectrum are

$$D^{R}_{m}(\mathbf{q},\omega) = (\omega - \Omega_q + i0)^{-1},\quad \Omega_q = Bq^2\ , \qquad (29)$$

where $B = \Theta_c/p_F^2$, and the Curie temperature $\Theta_c = aJ^2/\varepsilon_F$, $a\sim 1$.

The electron spectrum for each of the spin-split subbands is $\varepsilon_{\uparrow,\downarrow} = p^2/2m \mp JS$. The vertices $\lambda_{\downarrow\uparrow}$ and $\lambda_{\uparrow\downarrow}$ related to absorption and emission of magnons according to (25) equal $\lambda_{\downarrow\uparrow} = \lambda_{\uparrow\downarrow} = J(2S/N)^{1/2}$. The effective vertices $(\Lambda_{\uparrow\downarrow})^{k}_{ij}$ and $(\Lambda_{\downarrow\uparrow})^{k}_{ij}$, which take into account the impurity renormalization in the first order, are similar to the vertices Λ^{k}_{ij} for the electron-phonon interaction and may be obtained from (16) by substituting for ig_{ql} the quantities $\Lambda_{\uparrow\downarrow}$ and $\Lambda_{\downarrow\uparrow}$ given by

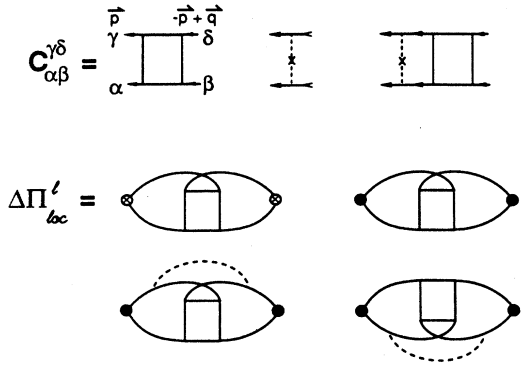

FIG. 5. Graphical equation for the cooperon and diagrams of $\Delta\Pi^{l}_{\mathrm{loc}}$ that take into account the effects of weak localization.

$$\Lambda_{\uparrow\downarrow} = -(\Lambda_{\downarrow\uparrow})^{*} = -J\left[\frac{S}{N}\right]^{1/2}\frac{i}{2ql}\ln\left[\frac{ql+\omega\tau+2JS\tau+i}{-ql+\omega\tau+2JS\tau+i}\right]\ . \qquad (30)$$

When $q_T \gg q_0$ and $q_T l \gg 1$, where $q_0 = 2JS/v_F$ and $Bq_T^2 = T$, the subband splitting may be neglected and we have

$$\Lambda_{\uparrow\downarrow} = \Lambda_{\downarrow\uparrow} = -J\left[\frac{S}{N}\right]^{1/2}\frac{\pi}{2ql}\ . \qquad (31)$$

The diagrams for the phonon self-energy are shown in Fig. 5. Similar to the case of the electron-thermal phonon interaction, we have two contributions to the sound attenuation due to the electron-magnon interaction: $\Delta\gamma_{e\text{-}m\text{-imp}}$ and $\Delta\gamma_{e\text{-}m}$. For longitudinal phonons it is convenient to express the result through the contribution from the fifth diagram,

$$(\Delta\gamma^{l}_{e\text{-}m\text{-imp}})_5 \equiv \Delta\gamma_m = -\frac{C\pi^2 SZm}{40M}\left[\frac{J}{\varepsilon_F}\right]^2\left[\frac{T}{\Theta_c}\right]^{3/2}(v_F k)^2\tau\ ,$$

$$C = -\int\frac{d\omega}{\sqrt{\omega}}f(\omega)\approx 2.5\ ,$$

$$(\Delta\gamma^{l}_{e\text{-}m\text{-imp}})_{1\text{-}3} = -\frac{4}{\pi^2}\Delta\gamma_m,\quad (\Delta\gamma^{l}_{e\text{-}m\text{-imp}})_4 = \frac{1}{\pi^2}\Delta\gamma_m\ , \qquad (32)$$

$$(\Delta\gamma^{l}_{e\text{-}m\text{-imp}})_{6\text{-}10} = \tfrac{4}{5}(\Delta\gamma^{l}_{e\text{-}m\text{-imp}})_{1\text{-}5}\ .$$

Combining all contributions mentioned above and performing a similar calculation for the transverse phonons, we get

$$\Delta\gamma^{l}_{e\text{-}m\text{-imp}} = \frac{9}{5}\left[1-\frac{3}{\pi^2}\right]\Delta\gamma_m\ ,$$

$$\Delta\gamma^{t}_{e\text{-}m\text{-imp}} = \frac{3}{4}\left[1-\frac{4}{\pi^2}\right]\Delta\gamma_m\ . \qquad (33)$$

Retaining terms of order q/p in the sound-phonon vertices, of the first diagram, we get the correction $\Delta\gamma_{e\text{-}m}$,

$$\Delta\gamma^{l}_{e\text{-}m}=-\frac{\pi^2 Z^2 S T^2 m\tau}{10C\Theta_c M}(kv_F)^2\tau,\quad \Delta\gamma^{t}_{e\text{-}m}=\tfrac{1}{36}\Delta\gamma^{l}_{e\text{-}m}\ . \tag{34}$$

For lower temperatures, $q_T \ll q_0$, and $2JS\tau \gg 1$,

$$\Lambda_{\uparrow\downarrow}=(\Lambda_{\downarrow\uparrow})^*=\frac{i}{2S\tau}\left[\frac{S}{N}\right]^{1/2}. \tag{35}$$

The straightforward calculation shows that all diagrams of Fig. 4 now mutually cancel. The finite result appears only after an expansion of the electron Green's function in powers of $q_T q_0^{-1} \ll 1$, and we have $\Delta\gamma_{e\text{-}m\text{-}\mathrm{imp}} \approx T^{5/2}$, and this may be neglected. This is similar to the cancellation in $\Delta\gamma_{e\text{-ph-imp}}$ for $q_T l \ll 1$ described in Sec. III. The same cancellation also takes place for $\Delta\sigma_{e\text{-ph-imp}}$ and $\Delta\sigma_{e\text{-}m\text{-imp}}$.[17] A typical value of J is $\approx 0.1\varepsilon_F$, and hence the inequality $q_T < q_0$ in a ferromagnetic metal is valid for temperatures $T < 10$ K.

IV. EFFECT OF WEAK LOCALIZATION

When calculating the corrections to the sound attenuation due to the effect of weak localization, we need to know the expression for the cooperon $C^{\gamma\delta}_{\alpha\beta}$ (Fig. 5) in the Keldysh-diagrammatic technique:

$$\begin{aligned}
&C^{12}_{12}=C^{21}_{21}=\frac{1}{\pi\nu\tau},\quad C^{\gamma\delta}_{22}=C^{22}_{\alpha\beta}=0\ ,\\
&C^{12}_{21}=(C^{21}_{12})^*=\frac{1}{\pi\nu\tau}\frac{1}{1-\zeta^*}\ ,\\
&C^{11}_{12}=-(C^{11}_{21})^*=\frac{1}{\pi\nu\tau}\frac{S(\varepsilon+\omega)\zeta}{1-\zeta}\ ,\\
&C^{12}_{11}=-(C^{21}_{11})^*=\frac{1}{\pi\nu\tau}\frac{S(\varepsilon)\zeta^*}{1-\zeta^*}\ ,\\
&C^{11}_{11}=-\frac{S(\varepsilon)S(\varepsilon+\omega)}{\pi\nu\tau}2\,\mathrm{Re}\left[\frac{\zeta\zeta^*}{1-\zeta}\right],
\end{aligned} \tag{36}$$

where

$$\begin{aligned}
\zeta\equiv\zeta(\mathbf{q},\Omega)&=\frac{1}{\pi\nu\tau}\int d\mathbf{p}\frac{1}{(2\pi)^3}G^A(\mathbf{p},\varepsilon)G^R(\mathbf{p}-\mathbf{q},\varepsilon+\Omega)\\
&=1+i\Omega\tau-Dq^2\tau\ .
\end{aligned} \tag{37}$$

For low frequency, $\Omega < 1/\tau_\varphi$, where τ_φ is the electron phase relaxation time, Ω in ζ should be substituted for $1/\tau_\varphi$. In further calculations, Ω represents the frequency of sound, $\omega_{k\lambda}$, and the temperature dependence of the sound attenuation appears when $\omega_{k\lambda}\tau_\varphi \ll 1$. Here, τ_φ is defined by some inelastic electron scattering—for example, the electron-phonon or electron-electron interactions. When τ_φ is defined by the spin-spin or spin-orbit interactions, the temperature dependence of the sound attenuation is absent.

The essential diagrams for the longitudinal-phonon self-energy are shown in Fig. 6. The last three diagrams containing vertices Γ_f mutually cancel. For transverse phonons we consider only the first diagram with vertices Γ_0, and as a result obtain

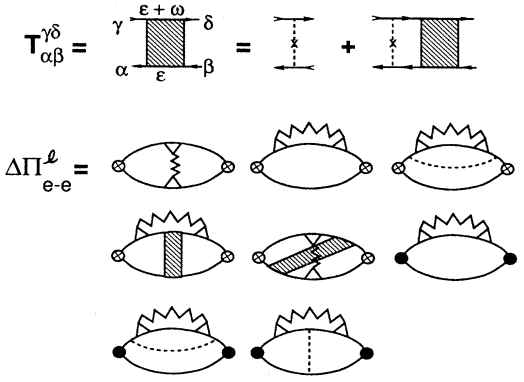

FIG. 6. Block T, which defines the impurity renormalization in the particle-hole channel. $\Delta\Pi^{l}_{e\text{-}e}$ describes the effects of the electron-electron interaction.

$$\Delta\gamma^{l}_{\mathrm{loc}}=-\frac{2\sqrt{3}Z}{5\pi}\frac{k^2}{M(\varepsilon_F\tau)}\left[\frac{\tau}{\tau_\varphi}\right]^{1/2},\quad \Delta\gamma^{t}_{\mathrm{loc}}=\tfrac{3}{4}\Delta\gamma^{l}_{\mathrm{loc}}\ . \tag{38}$$

The electron system may be considered two dimensional for films with thickness $d < (D\tau_\varphi)^{1/2}$. For phonons the situation is more complicated. The experimental feasibility of two-dimensional phonons is very questionable. Investigation of the attenuation of three-dimensional phonons on two-dimensional electrons in metal-oxide-semiconductor field-effect transistor structures[18] reveals many peculiarities of boundary effects that may obscure the localization and interaction effects. Layer compounds may be more appropriate for studying the effect of the low-dimensional electron system on the sound attenuation, but they demand special consideration. For this reason, we write the expressions for the attenuation of two-dimensional phonons on two-dimensional electrons, considering this case only as a model. As may be shown, the coefficient $\frac{2}{3}$ in g_{ql} given by (10) becomes 1, the factor $1-3x^2$ in (12) is replaced by $1-2x^2$, and the coefficient $\frac{4}{5}$ in (15) is replaced by $\frac{1}{2}$. As a result, we find

$$\Delta\gamma^{l}_{\mathrm{loc}}=\Delta\gamma^{t}_{\mathrm{loc}}=\frac{Z}{4\pi}\frac{k^2}{M}\ln(\tau_\varphi/\tau),\quad d=2\ . \tag{39}$$

V. ELECTRON-ELECTRON INTERACTION

In the Keldysh-diagrammatic technique the screened Coulomb potential has the same matrix structure as the G function. Below we write expressions for $V^R_{e\text{-}e}$ and $V^A_{e\text{-}e}$, which we need for further calculations:

$$\begin{aligned}
&V^R_{e\text{-}e}(\mathbf{q},\omega)=[V^A_{e\text{-}e}(\mathbf{q},\omega)]^*=\frac{V_0(q)}{\epsilon^R(,\omega)}\ ,\\
&V_0(q)=\frac{4\pi e^2}{q^2},\quad \epsilon^R(\mathbf{q},\omega)=1-V_0(q)P^R(\mathbf{q},\omega)\ ,\\
&P^R(\mathbf{q},\omega)=-\nu\left[1+\frac{i\omega\tau\zeta}{1-\zeta}\right],
\end{aligned} \tag{40}$$

where ζ is defined in (14). As a result, in the three- and

two-dimensional cases we have

$$V^R(\mathbf{q},\omega)=4\pi e^2\left[q^2+\frac{D\kappa_3^2 q^2}{-i\omega+Dq^2}\right]^{-1},$$
$$\kappa_3^2=4\pi e^2\nu_3,\quad \nu_3=mp_F/\pi^2,\quad d=3\ ;$$
$$V^R(\mathbf{q},\omega)=2\pi e^2\left[|q|+\frac{D\kappa_2 q^2}{-i\omega+Dq^2}\right]^{-1},\quad (41)$$
$$\kappa_2=2\pi e^2\nu_2,\quad \nu_2=m/\pi,\quad d=2\ .$$

We also write the expression for the vertex of the electron-electron interaction, renormalized by impurities, as shown in Fig. 1:

$$W_{22}^1=\frac{1}{\sqrt{2}(1-\zeta)},\quad W_{12}^1=\frac{S(\varepsilon)\zeta}{\sqrt{2}(1-\zeta)},$$
$$W_{21}^1=-\frac{S(\varepsilon+\omega)\zeta}{\sqrt{2}(1-\zeta)},\quad W_{22}^2=0,\quad W_{12}^2=W_{21}^2=\frac{1}{\sqrt{2}},\quad (42)$$
$$W_{11}^1=\frac{1}{\sqrt{2}}\left[\frac{1}{1-\zeta^*}-2S(\varepsilon)S(\varepsilon+\omega)\mathrm{Re}\left[\frac{\zeta}{1-\zeta}\right]\right],$$
$$W_{11}^2=\frac{[S(\varepsilon+\omega)-S(\varepsilon)]\zeta^*}{1-\zeta^*}.$$

For the block of impurity ladders in the diffusion channel, we have

$$T_{21}^{12}=T_{12}^{21}=\frac{1}{\pi\nu\tau},\quad T_{22}^{\gamma\delta}=T_{\alpha\beta}^{22}=0,$$
$$T_{12}^{12}=(T_{21}^{21})^*=\frac{1}{\pi\nu\tau}\frac{1}{1-\zeta},$$
$$T_{12}^{11}=-(T_{21}^{11})^*=\frac{-S(\varepsilon+\omega)}{\pi\nu\tau}\frac{\zeta}{1-\zeta},\quad (43)$$
$$T_{11}^{12}=-(T_{11}^{21})^*=\frac{S(\varepsilon)}{\pi\nu\tau}\frac{\zeta}{1-\zeta},$$
$$T_{11}^{11}=-\frac{S(\varepsilon)S(\varepsilon+\omega)}{\pi\nu\tau}2\,\mathrm{Re}\left[\frac{\zeta}{1-\zeta}\right].$$

Expressions (42) and (43), together with the rules described in Sec. II, allow one to calculate easily all exchange diagrams of the electron-electron interaction $\Delta\Pi_{e\text{-}e}^l$, shown in Fig. 6. The contributions of the first three diagrams add up to zero. A similar cancellation also occurs in the corresponding diagrams for the conductivity. For the conductivity, when the contribution of the fifth and sixth diagrams are calculated, the electron Green's functions to the left and right of the block $T_{\alpha\beta}^{\gamma\delta}$ should be expanded to first order in $\mathbf{q}\cdot\mathbf{v}$. For the longitudinal phonons a nonzero result for the fifth and sixth diagrams arises only when we expand G functions to second order in the parameters $\mathbf{q}\cdot\mathbf{v}$ or $\mathbf{k}\cdot\mathbf{v}$, and so the result is very small. Now we consider the diagrams containing the vertices Γ_f, which were omitted in Refs. 8–10. The tensor-index structure of the vertex Γ_f leads to only the last three diagrams of Fig. 6. It may be shown that they mutually cancel.

For the transverse sound we substitute vertices Γ_0 for

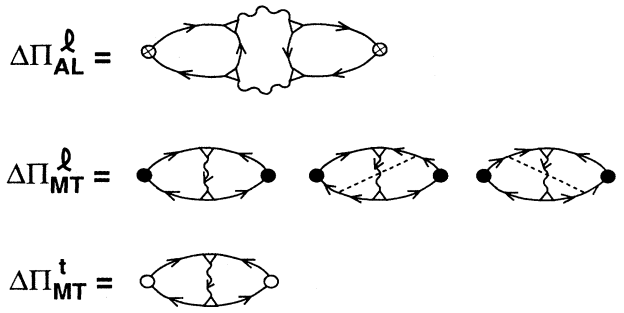

FIG. 7. Phonon self-energies which describe the effect of the electron-electron interaction in the Cooper channel on the sound attenuation. The wavy line is the fluctuation propagator.

Γ_s in the first five diagrams of Fig. 6. The first three diagrams mutually cancel in the same way as for the longitudinal sound. The fourth and fifth diagrams vanish after the angular integration, and the expansion of electron Green's functions over $\mathbf{q}\cdot\mathbf{v}$ and $\mathbf{k}\cdot\mathbf{v}$ cannot change this result, so $\Delta\gamma_{e\text{-}e}^t=0$.

Now we consider the interaction effect in the Cooper channel on the sound attenuation. We start with the Aslamazov-Larkin diagram for the longitudinal sound. The requirement of the impurity renormalization of the interaction vertices for the fluctuation propagator leads to the diagram $\Delta\Pi_{\mathrm{AL}}^l$ with the sound vertices Γ_s shown in Fig. 7. Thus we have to expand the electron Green's function in each block of three electron Green's function to second order in the parameters $\mathbf{q}\cdot\mathbf{v}$ or $\mathbf{k}\cdot\mathbf{v}$. As a result, the Aslamazov-Larkin correction to the sound attenuation occurs less than the corresponding correction to the conductivity $\Delta\sigma_{\mathrm{AL}}$:

$$\frac{\Delta\gamma_{\mathrm{AL}}^l}{\gamma^l}\ll\frac{\Delta\sigma_{\mathrm{AL}}}{\sigma},\quad \Delta\gamma_{\mathrm{AL}}^t=0,\quad (44)$$

where σ is the dc conductivity. We can construct the Aslamazov-Larkin diagram with the scalar vertices Γ_f if we do not renormalize the interaction vertices for one of the fluctuation propagators, but the result is also small.

The analyses shows that the anomalous contribution from the Maki-Thompson diagram appears only for the diagrams with the sound vertices Γ_f, as shown in Fig. 7. However, all these diagrams mutually cancel. This result coincides with Ref. 19. However, for the transverse sound we have only one Maki-Thompson diagram, $\Delta\Pi_{\mathrm{MT}}^t$ (see Fig. 7), and, as a result,

$$\frac{\Delta\gamma_{\mathrm{MT}}^t}{\gamma^t}=\frac{\Delta\sigma_{\mathrm{MT}}}{\sigma},\quad \Delta\gamma_{\mathrm{MT}}^l=0,\quad (45)$$

where $\Delta\sigma_{\mathrm{MT}}$ is the corresponding correction to the conductivity. Equation (45) is valid for any dimensions and also in the presence of magnetic field.

VI. SUMMARY

The effective vertices Γ_s and Γ_f that take into account the screening effects and the impurity renormalization allowed us to calculate the effect of different kinds of elec-

tron interactions on the sound attenuation. Note that for the electron-phonon and electron-magnon interactions the correction to the sound attenuation is proportional to the corresponding corection to the conductivity, $\Delta\gamma \sim \Delta\sigma$. For the localization effects, $\Delta\gamma_{\rm loc} \sim -\Delta\sigma_{\rm loc}$, and there is no effect of the Coulomb electron-electron interaction on the sound attenuation. The effect of the interaction in the Cooper channel on the longitudinal sound is very weak, but there is a correction to the transverse sound attenuation proportional to the Maki-Thompson correction to the conductivity. We point out that all corrections to the sound attenuations are proportional to k^2 (not to ω_k^2), and in this form are also applicable to optical phonons.[20]

ACKNOWLEDGMENTS

The author is very grateful to D. Belitz, A. Kapitulnik, V. Kalmeyer, A. V. Sergeev, and A. A. Varlamov for very valuable discussions. This work was supported by the U.S. National Science Foundation under Grant No. DMR-85-19753.

[1]A. B. Pippard, Philos. Mag. **46**, 1104 (1955).
[2]A. Schmid, Z. Phys. **259**, 421 (1973).
[3]G. Grunevald and K. Sharnberg, Z. Phys. **268**, 197 (1974); B **20**, 61 (1975).
[4]A. B. Bhatia and R. A. Moore, Phys. Rev. **121**, 1075 (1961).
[5]G. G. Natale and I. Rudnick, Phys. Rev. **167**, 687 (1968).
[6]B. L. Altshuler and A. G. Aronov, Zh. Eksp. Teor. Fiz. **75**, 1616 (1978) [Sov. Phys.—JETP **48**, 812 (1978)].
[7]M. Yu. Reizer and A. V. Sergeev, Zh. Eksp. Teor. Fiz. **92**, 2291 (1987) [Sov. Phys.—JETP **65**, 1291 (1987)].
[8]A. Houghton and H. Won, J. Phys. C **18**, L507 (1985).
[9]G. Kotliar and T. V. Ramakrishnan, Phys. Rev. B **31**, 8188 (1985).
[10]T. R. Kirkpatrick and D. Belitz, Phys. Rev. B **34**, 2168 (1986); **34**, 9008 (1986).
[11]C. Castelani and G. Kotliar, Phys. Rev. B **34**, 9012 (1986); **36**, 7407 (1987).
[12]L. V. Keldysh, Zh. Eksp. Teor. Fiz. **47**, 1514 (1964) [Sov. Phys.—JETP **20**, 1018 (1965)].
[13]E. I. Blount, Phys. Rev. **114**, 418 (1959).
[14]T. Tsuneto, Phys. Rev. **121**, 402 (1961).
[15]M. Yu. Reizer and A. V. Sergeev, Zh. Exp. Teor. Fiz. **90**, 1056 (1986) [Sov. Phys.—JETP **63**, 616 (1986)].
[16]S. V. Vonsovskii, *Magnetism* (Halsted, New York, 1975).
[17]The result of Ref. 7 for conductivity for $q_T < q_0$ was corrected by A. V. Sergeev, Ph.D. thesis, Moscow State University, 1987 (unpublished).
[18]J. C. Hensel, R. C. Dynes, and D. C. Tsui, Phys. Rev. B **28**, 1124 (1983); J. C. Hensel, B. I. Halperin, and R. C. Dynes, Phys. Rev. Lett. **51**, 2302 (1983).
[19]L. G. Aslamazov and A. A. Varlamov, Zh. Eksp. Teor. Fiz. **77**, 2410 (1979) [Sov. Phys.—JETP **50**, 1164 (1979)].
[20]M. Yu. Reizer, Phys. Rev. **38**, 10398 (1988).